Archival Report

Biological Psychiatry: CNNI

Non-negative Matrix Factorization Reveals Resting-State Cortical Alpha Network Abnormalities in the First-Episode Schizophrenia Spectrum

Henry Phalen, Brian A. Coffman, Avniel Ghuman, Ervin Sejdić, and Dean F. Salisbury

ABSTRACT

BACKGROUND: Little is known about neural oscillatory dynamics in first-episode psychosis. Pathophysiology of functional connectivity can be measured through network activity of alpha oscillations, reflecting long-range communication between distal brain regions.

METHODS: Resting magnetoencephalographic activity was collected from 31 individuals with first-episode schizophrenia spectrum psychosis and 22 healthy control individuals. Activity was projected to the realistic cortical surface, based on structural magnetic resonance imaging. The first principal component of activity in 40 Brodmann areas per hemisphere was Hilbert transformed within the alpha range. Non-negative matrix factorization was applied to single-trial alpha phase-locking values from all subjects to determine alpha networks. Within networks, energy and entropy were compared.

RESULTS: Four cortical alpha networks were pathological in individuals with first-episode schizophrenia spectrum psychosis. The networks involved the bilateral anterior and posterior cingulate; left auditory, medial temporal, and cingulate cortex; right inferior frontal gyrus and widespread areas; and right posterior parietal cortex and widespread areas. Energy and entropy were associated with the Positive and Negative Syndrome Scale total and thought disorder factors for the first three networks. In addition, the left posterior temporal network was associated with positive and negative factors, and the right inferior frontal network was associated with the positive factor.

CONCLUSIONS: Machine learning network analysis of resting alpha-band neural activity identified several aberrant networks in individuals with first-episode schizophrenia spectrum psychosis, including the left temporal, right inferior frontal, right posterior parietal, and bilateral cingulate cortices. Abnormal long-range alpha communication is evident at the first presentation for psychosis and may provide clues about mechanisms of dysconnectivity in psychosis and novel targets for noninvasive brain stimulation.

Keywords: Alpha, Machine learning, Magnetoencephalography, Network, Non-negative matrix factorization, Schizophrenia

https://doi.org/10.1016/j.bpsc.2019.06.010

Schizophrenia is associated with disabling symptoms, including visual and auditory hallucinations, blunted emotion, and deficiencies in attention, decision making, and working memory. The disorder is often chronic and typically emerges during late adolescence and young adulthood. The exact pathology remains unknown, and its explication is complicated by the progressive course of the disorder (1–3) and the cumulative effects of secondary illness-related factors. These confounds are ameliorated by studying individuals near the emergence of psychosis within the schizophrenia spectrum. Definitive diagnoses cannot always be made at the first episode. Hence, the schizophrenia spectrum at first episode includes schizophrenia, schizoaffective disorder, schizophreniform disorder, delusional disorder, and psychosis not otherwise specified.

Schizophrenia involves dysconnection between neural regions (4–6). Functional connectivity is reduced in schizophrenia (7–11), and this reduction may have an anatomical component (12–14). For example, schizophrenia is associated with reduced structural connectivity in several polymodal hubs and so-called rich clubs, centralized hubs at the top of the cortical processing hierarchy (15). This dysconnection is also evident in functional activity. Electroencephalography (EEG) and magnetoencephalography (MEG) reflect summed dendritic fields and provide a high-resolution window into real-time neural network activity. MEG allows greater spatial resolution of the cortical sources of neural oscillations because magnetic fields, unlike electric fields, are unaffected by intervening tissue boundaries. In combination with accurate sulcal-gyral models

ISSN: 2451-9022

of individual head shape based on structural magnetic resonance imaging (MRI), MEG activity can be source resolved to the cortical surface with reasonable spatial resolution of 5 to 10 mm.

Neural oscillations have a known role in coordinating activity in both local brain networks (16) and networks connecting brain regions over long distances (17). Changes in overall oscillatory activity are observed in schizophrenia (18). Distributed oscillatory networks are characterized through spectral frequency phase relationships between cortical regions. The alpha rhythm, thought to reflect in part information transfer between distal brain regions (19,20), is reduced in schizophrenia (11,21).

Alpha power was traditionally associated with vigilance and sustained attention, representing an underlying idle state of the brain. For example, alpha increases when the eyes are closed and diminishes when the eyes are open (22,23). However, alpha has a role in working memory (24–26) and top-down control (27–30). Alpha phase affects the synchrony of neuronal activity both locally and between regions of the brain (31). In addition, alpha activity acts to suppress task-irrelevant processing (31), activate task-relevant processing (29), or both (29,32). Thus, in addition to reflecting the general idling of cortical areas, alpha likely plays a role in long-range communication between distal cortical areas.

In that regard, long-distance synchrony in gamma activity between distal cortical areas likely involves alpha oscillations that coordinate between areas (33–36). Importantly, attention effects are associated not only with the alpha-gamma power anticorrelation but also with cross-frequency coupling. Gamma band bursts entrain to alpha phase, such that sensory gamma bursts become locally organized via prefrontal cortex (PFC)–controlled alpha modulations (37). Thus, alpha plays a role in modifying sensory processing via input from executive and other distributed areas. Therefore, we selectively targeted alpha oscillations for analysis of distributed networks because alpha is a biologically viable, empirically demonstrated coordinating frequency between distal cortical areas.

We used alpha phase locking (38) as an indicator of functional connectivity between regions during the resting state. We assume that there are multiple overlapping networks within the brain that contribute to the observed signal. Thus, we employed a machine learning clustering technique, nonnegative matrix factorization (NMF), to subdivide phase synchrony graphs into functional networks. NMF, traditionally used in applications such as image recognition (39), genetics (40), and natural language detection (41), has previously been used to investigate neural differences between subject groups using functional MRI (42). We determined the energy and entropy of these networks to provide network-specific information on alpha irregularity in schizophrenia. Energy measures the overall quantity of information transfer in a system and is akin to the power of the signal that is being communicated. Entropy represents the order/disorder of communication and information transfer within each network and measures the degree of complexity in the neural signal. We specifically aimed to determine networks of interest by relatively light, data-driven computational methods to identify promising network features for future in-depth studies of pathology in early-course psychosis and for potential development of optimal patient-specific precision medicine treatments targeting specific circuits.

METHODS AND MATERIALS

Participants were 31 subjects with first-episode schizophrenia (FESz) and 22 healthy control (HC) subjects, group matched for age, sex, and estimated premorbid IQ. Subjects with FESz and HC subjects differed on socioeconomic status and Measurement and Treatment Research to Improve Cognition in Schizophrenia overall scores, consistent with the deleterious effects of psychosis on functioning and cognition. Parental socioeconomic status was significantly lower in subjects with FESz. (Note that none of the energy or entropy measures reported below correlated with parental socioeconomic status in either group.) Seven subjects with FESz were unmedicated. See Table 1 for demographic and clinical data. This study was approved by the University of Pittsburgh Institutional Review Board. All subjects provided informed consent and were paid for participation.

Five minutes of eyes-open resting MEG data were collected in a magnetically shielded room. We acquired resting-state data with eyes open because we were interested in entropy measures of network-level activity, and spectral entropy is greatest in eyes-open EEG (43). Both EEG and MEG were recorded, but only the resting MEG is reported here. MEG data

Table 1. Subject Demographic and Clinical Data

	FESz	HC	*p*
n (Male/Female)	31 (20/11)	22 (13/9)	.69
Age, Years	21.7 (5.0)	21.7 (3.7)	.96
SES	26.9 (13.2)	33.4 (12.5)	.05[a]
Parental SES	39.6 (14.0)	53.3 (7.6)	<.001[a]
WASI IQ	104.9 (15.2)	106.4 (8.6)	.69
MATRICS	35.0 (16.6)	49.1 (6.4)	<.001[a]
GAS	38.1 (9.2)		
SAPS	6.6 (3.3)		
SANS	10.3 (3.1)		
PANSS Total	76.5 (15.0)		
PANSS Pos	19.4 (5.7)		
PANSS Neg	17.3 (4.8)		
PANSS TD	11.2 (3.2)		
Medication[b]	205.5 (160.1)		
DUP, Weeks	36		

Subject *n* and sex distributions are number of individuals. Duration of untreated psychosis (DUP) is median value. All other values are mean (SD).

FESz, subjects with first-episode schizophrenia spectrum; GAS, Global Assessment Scale; HC, healthy control subjects; MATRICS, Measurement and Treatment Research to Improve Cognition in Schizophrenia Consensus Cognitive Battery composite score; Neg, negative factor score; PANSS, Positive and Negative Syndrome Scale; Pos, positive factor score; TD, thought disorder factor score; Total, total score; SANS, Scale for the Assessment of Negative Symptoms global score; SAPS, Scale for the Assessment of Positive Symptoms global score; SES, socioeconomic status; WASI IQ, Wechsler Abbreviated Scale of Intelligence score.

[a]Significant effect.

[b]Medication in chlorpromazine equivalents [oral dosages from Andreasen *et al*. (74); depot dosages from Gardner *et al*. (75)].

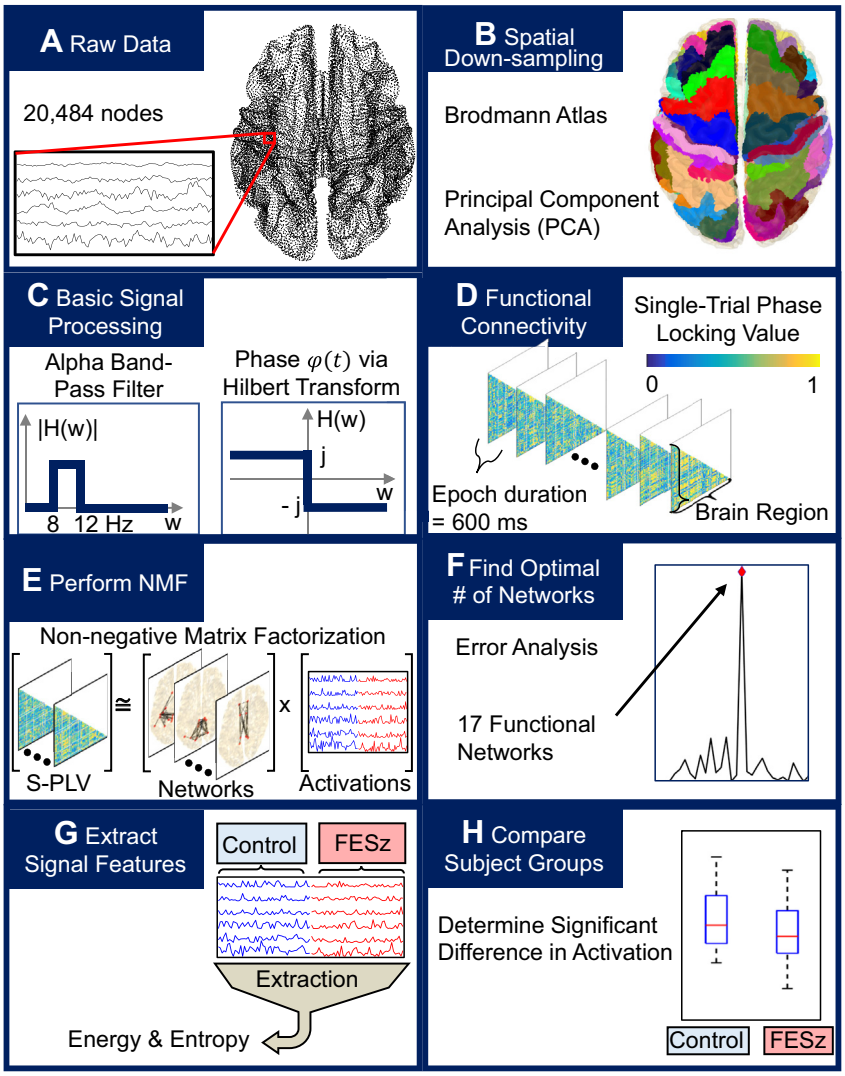

Figure 1. Processing pipeline. **(A–C)** Magnetoencephalography data **(A)** were spatially down-sampled into Brodmann areas using principal component analysis (PCA) **(B)**, bandpass filtered into the alpha band, and transformed into the analytic signal using the Hilbert transform **(C)**. **(D)** Analytic signal phases were compared using single-trial phase-locking values (S-PLV) to generate functional connectivity graphs in a windowed manner for each subject. **(E)** Non-negative matrix factorization (NMF) was used iteratively to determine networks. **(F)** The optimal number of networks was determined using error analysis. **(G, H)** Finally, energy and entropy measurements associated with each network for every subject were determined **(G)** and compared between healthy control and first-episode schizophrenia spectrum (FESz) groups **(H)**.

were recorded using a 306-channel whole-head MEG system (Elekta Neuromag; Elekta Instrument, Helsinki, Finland) with a sampling rate of 1000 Hz (online bandpass filter = 0.1–330 Hz). Bipolar leads were placed above and below the left eye and lateral to the outer canthi of both eyes. Bipolar electrocardiogram leads were placed just below the left and right clavicle. Four head position indicator coils were placed between electrodes on the surface of the EEG cap, and locations (relative to the nasion and preauricular points) were recorded using a three-dimensional digitizer (ISOTRAK; Polhemus, Colchester, VT). Head position was tracked continuously throughout the experiment. Subjects were instructed to fixate on a central cross for the duration of the test.

Structural MRI was obtained for use in MEG source modeling. Sagittal T1-weighted anatomical MR images were obtained using a Siemens (Munich, Germany) TIM Trio 3T MRI system with a multiecho three-dimensional magnetization prepared rapid acquisition gradient-echo sequence (repetition time = 2530 ms; echo times = 1.74, 3.6, 5.46, 7.32 ms; inversion time = 1260 ms; flip angle = 7°; field of view = 220 × 220 mm; isotropic voxel size = 1 mm; 176 slices; generalized autocalibrating partially parallel acquisition acceleration factor = 2).

Head movement correction was completed using Elekta MaxMove, and external noise was reduced via the temporal extension of signal space separation (44) implemented in Elekta MaxFilter. Eyeblink and heartbeat artifacts were removed using adaptive mixture independent component analysis (45,46) implemented in EEGLab (https://sccn.ucsd.edu/eeglab/index.php). The MEG sensor locations were registered to structural images using MRILab (Elekta Neuromag Oy, Helsinki, Finland). The locations of sources were constrained to the gray/white matter boundary segmented from the structural MRI data using FreeSurfer (http://www.surfer.nmr.mgh.harvard.edu). This boundary was tessellated into an icosohedron with 5-mm spacing between vertices, resulting in ~5000 current locations per hemisphere. A forward solution for vertices was modeled as a single sphere.

Source activity was then estimated from 204 planar gradiometers using minimum norm estimation (47). The noise covariance matrix and forward solution were used to create a linear inverse operator using a loose orientation constraint of 0.4 (48) with depth weighting applied. Sensor covariance was estimated from MEG data collected without a subject in the magnetically shielded room on the same day as resting-state acquisition. Data from individual subjects were then morphed into a standard space prior to functional connectivity analysis with 5-mm smoothing.

For data reduction, following MEG cortical surface source projection, the cortical surface was parcellated into 80 Brodmann areas (BAs) (see processing pipeline in Figure 1). The first principal component across the spatial dimension of the signals from each area was used to represent regional cortical activity. These 80 component signals were bandpass filtered into the alpha band (8–12 Hz) using a 20th-order Butterworth bandpass filter applied bidirectionally to achieve zero-phase filtering. Nominal break frequencies were chosen so that after the zero-phase filtering, the true break frequencies would be at 8 and 12 Hz. Synchrony was estimated between phases of alpha for each pair of BAs using single-trial phase-locking values (S-PLVs) (38). The calculation of S-PLV results in lower temporal resolution when compared with multitrial PLV but is appropriate for estimating phase locking between resting-state signals that lack event-initiated epochs. S-PLV is defined as

$$\mathrm{S-PLV}(t) = \left| \frac{1}{\delta} \int_{t-\frac{\delta}{2}}^{t+\frac{\delta}{2}} e^{-j(\phi_1(\tau)-\phi_2(\tau))} d\tau \right|$$

where δ is the width of the window, typically chosen between 6 and 10 times the length of the midband period (38). Nonoverlapping windows of 600 ms were chosen, corresponding to δ=6 times the mid-alpha-band period of 100 ms. The instantaneous phase ϕ of component signals was taken to be the phase of the analytic signal obtained using the Hilbert transform (49). These S-PLVs were then used to create a weighted, undirected connectivity graph *C* for each time window (50). The nodes of *C* correspond to BAs, and the edges represent the S-PLVs, taken to be the functional connectivity, between pairs of BAs. In total, *T* connectivity graph matrices *C* of size $b \times b$ are generated for each *S* subjects, where *T, S,* and *b* are the numbers of time windows per subject, subjects, and BAs, respectively.

To extract information from these connectivity graphs, the NMF technique was used. NMF is an unsupervised machine learning algorithm that can be used to decompose an input matrix *A* into two components: a matrix *W* of bases, or subgraphs, and a matrix *H* of their corresponding contributions to the input matrix *A* (39). Connectivity graphs were combined to serve as the input matrix (*A*) for NMF that yielded subgraphs (*W*), taken to be functional resting-state alpha networks, and associated time series of contributions (*H*), taken to be the relative temporal activation of each of these networks. Because the synchrony graphs are undirected, all functional relationships were described in a single input matrix A by unwrapping and concatenating the lower triangular of each S-PLV connectivity graph *C,* resulting in matrix *A* having dimensions $b \times (b-1)/2 \times N$, where *N* is the number of time windows over all subjects, *S* multiplied by *T.*

Factorization was completed using the sparse, alternating non-negativity constrained least squares approach (51) that is given by the following minimization:

$$\min_{W,H} \frac{1}{2} \left\{ \|A - WH\|_F^2 + \eta \|W\|_F^2 + \beta \sum_{c=1}^{N} \|H(:,c)\|_1^2 \right\}, s.t. W, H \geq 0,$$

where $\|X\|_F$ is the Frobenius norm given by $\sqrt{\sum_{i=1}^{m}\sum_{j=1}^{n}|X_{ij}|^2}$, $\|\cdot\|_1$ is the ℓ_1- norm given by $\sum_{i=1}^{n}|X_i|$, and $H(:, c)$ is the *c*th column of *H.* Parameters β and η act to regulate the values in the subgraphs *W* and activations *H,* ensuring sparsity of the result while bounding the size of output values. The choice of β as 0.01 and η as the square of the maximum value in *A* was used because these have been shown to be robust values for these parameters (42,52). The sizes of *W* and *H* are $[b \times (b-1)/2 \times k]$ and $(k \times N)$, respectively, where *k* is the number of functional networks, which was chosen by performing NMF iteratively for increasing values of *k* and selecting the inflection point, or elbow, in the reconstruction residual sum of squares error curve (51) (Figure 2A). This is the point after which increasing the number of functional networks yields diminishing returns on model fit. Computationally, this was taken to be the point of first large change in curvature (Figure 2B) or, more specifically, the point at which the smallest ratio of the curvature to previous curvatures was maximized (Figure 2C). This method was intended to provide a repeatable and conservative way to prevent overfitting of the model.

The NMF algorithm was initialized using non-negative double singular value decomposition, which allows for improved factorization speed and provides stable outputs (53). Non-negative double singular value decomposition is best implemented on sparse inputs, and rather than apply an arbitrary threshold, sparsity of connectivity graphs *C* was obtained using a threshold from surrogate data analysis. The threshold was taken to be the 95th percentile of the maximum S-PLV generated from 500 pairs of independent white-noise surrogate signals. Previous studies including measures of synchrony have used white-noise surrogates to determine thresholds and have shown this method to be equivalent to other, more computationally heavy methods such as trial-shifted and phase-shuffled surrogates (54,55). Connectivity above what is seen in the surrogate data is likely to be real, not just the result of noise or random chance. Thus, this method identifies a reasonable threshold value above which connectivity is unlikely to reflect the result of random error or noise.

The energy and entropy of the activations associated with each functional network were calculated for individual subjects (42). The energy of a given network, which represents overall activation, was calculated as

$$\mathrm{Energy} = \sum_{i=1}^{N} w_i^2$$

where *N* is the length of the activation vector *w*. The functional network entropy, which quantifies the dynamics of

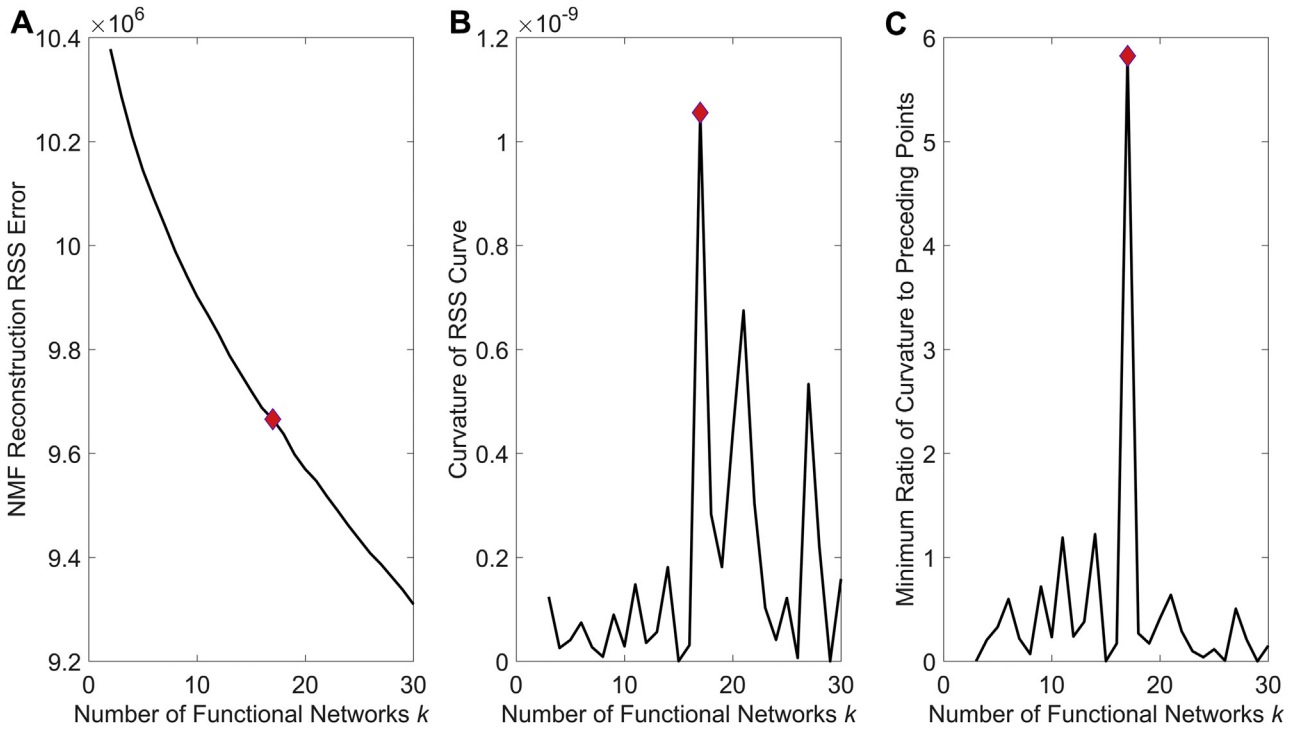

Figure 2. Method for determining number of functional networks. **(A)** The optimal number of functional networks occurs at the inflection point of the reconstruction residual sum of squares (RSS) error curve generated from iterative runs of non-negative matrix factorization (NMF) with increasing numbers of functional networks. **(B, C)** This point can be determined as the first point with a large change in curvature **(B)** or, most apparently, as the point at which the minimum ratio of curvature to the curvature at previous points is greatest **(C)**. These points are represented by red diamonds that correspond to 17 functional networks.

activation, was then calculated using the histogram-based method (56) as

$$\text{Entropy} = \sum_{i=1}^{N} -P(x_i) \log P(x_i)$$

where $P(x)$ is the probability function derived from the histogram. Because the measures were not normally distributed (maximum kurtosis > 30 for each measure), the energy and entropy of functional network activations were compared between subjects with FESz and HC subjects using the Wilcoxon rank-sum test. Because this is the first examination of alpha functional networks derived in this fashion, we adopted more liberal initial exploratory analyses, where $p < .05$ was considered meaningful; however, these data were also corrected for multiple comparisons with the Benjamini-Hochberg procedure with a false discovery rate of .15. To demonstrate the utility of factorization in the analysis, these energy and entropy calculations and comparisons were also performed on the data after filtering into the alpha band (i.e., prior to phase synchrony estimates). A correlation between whole-brain signal power (sum of the magnitude of the Fourier transform across regions) was also performed. These whole-brain analyses were similarly not normally distributed, so comparisons between subject groups were also made using the Wilcoxon rank-sum test.

Correlations between network activation measures and symptoms were investigated with Spearman's rank order correlations. Owing to the large number of possible correlations between energy and entropy for separate functional networks and individual symptoms, clinical measures were reduced to total, positive, negative, and thought disorder factors of the Positive and Negative Syndrome Scale. (Significant associations with items are presented in the Supplement, but caution must be used in interpretation.)

RESULTS

No significant difference between subject groups was observed in whole-brain alpha energy ($p = .203$), entropy ($p = .401$), or power ($p = .267$). Using NMF, 17 functional networks (Supplemental Figure S1) were determined. Comparisons between groups revealed four functional networks that exhibited significantly lower median energy in subjects with FESz, one of which survived correction for multiple comparisons (Figure 3). These were network 6, which consists primarily of distributed alpha coherence in the cingulate cortex; network 12, which connected the left hemisphere auditory cortex with the left medial temporal lobe and posterior cingulate; network 13, which consists of a hub in the right inferior frontal cortex Broca's homologue (BAs 44 and 45) hub with widespread connectivity (bilateral cingulate, bilateral lateral and medial temporal lobes, right hemisphere PFC, and bilateral

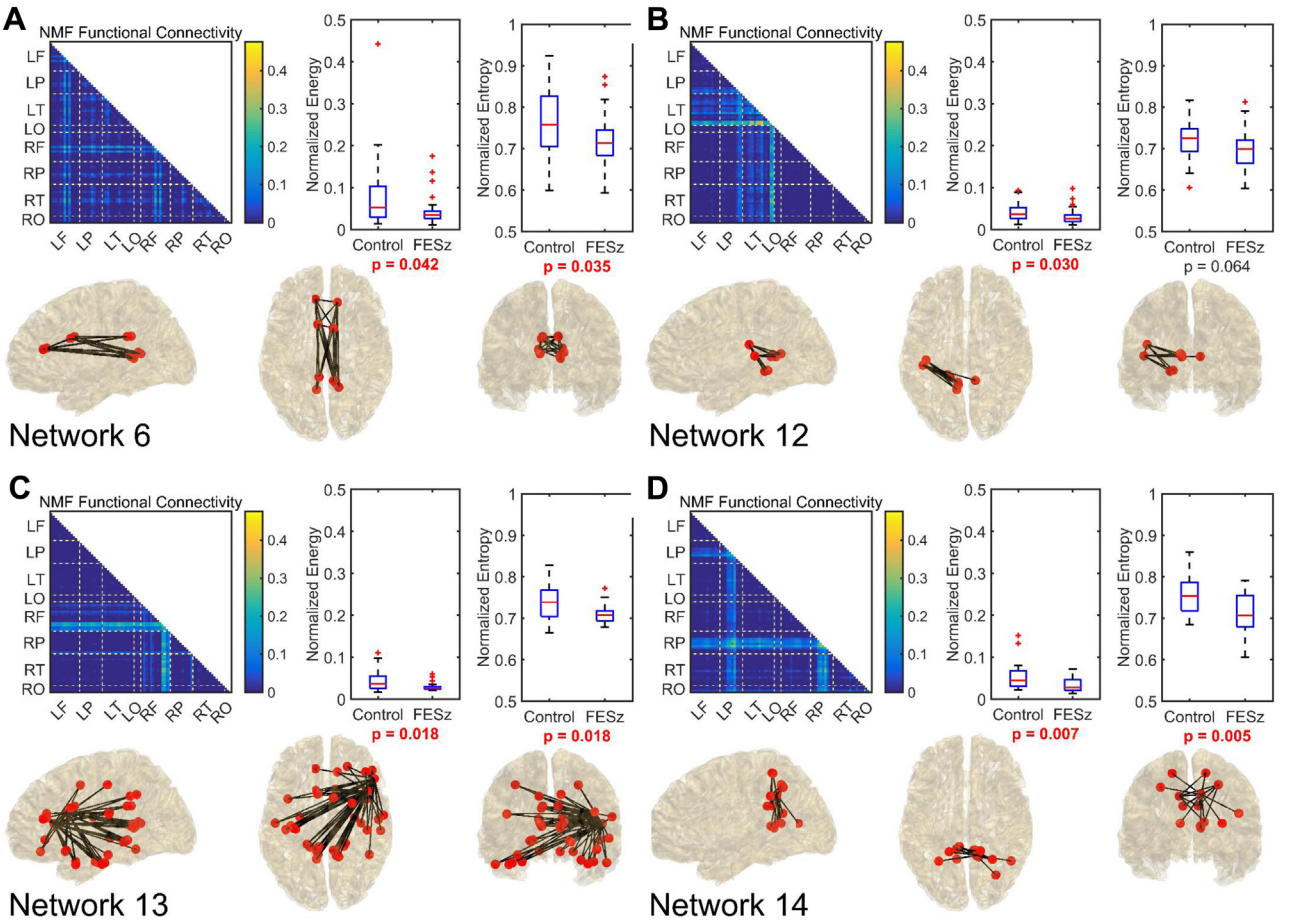

Figure 3. The four networks that differentiated healthy individuals from individuals with first-episode schizophrenia spectrum (FESz). Networks are represented as a connectivity graph and anatomically on a brain model: **(A)** network 6; **(B)** network 12; **(C)** network 13; **(D)** network 14. Healthy control and FESz group comparisons of energy and entropy are also provided. In the connectivity graph, each pixel represents a phase-locking relationship between two Brodmann areas. Values closer to the diagonal represent local communication, while values in the lower left represent cross-hemisphere communication. To further improve an anatomical understanding, dashed lines divide Brodmann areas from different lobes and are identified at the axes by their hemisphere (R, right; L, left) and lobe (F, frontal; P, parietal; T, temporal; O, occipital). The top third of connections by strength are also shown within the brain at sagittal, axial, and coronal views. FieldTrip software (73) was used in generation of these brain visuals. Energy and entropy values have been normalized between highest and lowest observed values across subjects, and the *p* value associated with the Wilcoxon rank-sum test is given. Comparisons with $p < .05$ are in bolded red text. NMF, non-negative matrix factorization.

sensorimotor cortex); and network 14, a network between the posterior cingulate cortex and bilateral superior parietal lobules. Of these four networks, the cingulate network, right inferior frontal network, and posterior cingulate superior parietal network also showed significant decreases in median activation entropy in subjects with FESz. Changes in both entropy and energy of the posterior cingulate superior parietal network survived correction for multiple comparisons.

Within HC subjects, energy and entropy measures across networks were highly correlated (ρs = .48–.99, all *p*s $< .05$). In subjects with FESz, energy and entropy were correlated among most networks, although network 6 (bilateral cingulate) and network 14 (posterior cingulate and bilateral superior parietal cortex) were uncorrelated. In subjects with FESz, there were widespread correlations between both energy and entropy measures and clinical symptoms for all networks except network 14 (posterior cingulate and bilateral superior parietal cortex) (see Table 2 and Supplemental Table S2). Lower energy and entropy in network 6 (bilateral cingulate) were associated with more total symptoms and greater thought disorder. Lower energy and entropy in network 12 (left posterior temporal) was associated with more total, positive, and negative symptoms and with greater thought disorder. Lower energy and entropy in network 13 (right inferior frontal) were associated with more total and positive symptoms and with greater thought disorder.

DISCUSSION

Using a data-driven approach to source-level functional connectivity analysis in alpha-band MEG data, we identified 17 discrete distributed functional networks based on phase locking (Supplemental Figure S1). From the analytical side, the observation that NMF extracts reasonable brain networks from connectivity graphs is an important methodological advance.

Table 2. Spearman's Correlations of Energy and Entropy With Clinical Measures

	Bilateral Cingulate (Network 6)		Left Posterior Temporal (Network 12)		Right Inferior Frontal (Network 13)		Posterior Cingulate Parietal (Network 14)	
	NRG	ENT	NRG	ENT	NRG	ENT	NRG	ENT
Between-Group Differences								
z Score	2.03	2.10	2.36	2.37	2.35	2.37	2.68	2.82
p Value	.04[a]	.04[a]	.03[a]	.06	.02[a]	.02[a]	.01[b]	.005[b]
Correlations With Symptoms								
PANSS total score								
Spearman's ρ	−.40	−.40	−.60	−.61	−.38	−.43	−.10	−.08
p Value	.04[b]	.04[b]	.001[b]	.001[b]	.06	.03[b]	.61	.69
PANSS positive factor score								
Spearman's ρ	−.35	−.30	−.46	−.45	−.42	−.42	−.18	−.19
p Value	.08	.14	.02[b]	.02[b]	.03[b]	.03[b]	.38	.35
PANSS negative factor score								
Spearman's ρ	−.22	−.23	−.54	−.56	−.15	−.22	−.15	−.13
p Value	.29	.25	.005[b]	.003[b]	.46	.29	.48	.52
PANSS thought disorder factor score								
Spearman's ρ	−.46	−.40	−.54	−.50	−.61	−.66	−.25	−.24
p Value	.02[b]	.04[b]	.004[b]	.009[b]	.001[b]	<.001[b]	.21	.23

PANSS item scores follow factor scores.
ENT, entropy; NRG, energy; PANSS, Positive and Negative Syndrome Scale.
[a]Significant *p* value ($p \leq .05$).
[b]Significant correlation ($p < .05$) surviving correction for multiple comparisons (false discovery rate = .15).

From the clinical neuroscience side, that several of these data-driven alpha networks were abnormal in subjects with FESz is an important new lead in understanding the pathophysiology of the disorder.

Four distributed networks (Figure 3) displayed lower energy in subjects with FESz, indicating less coherent alpha activation. The entropy decreases in three of these networks (networks 6, 13, and 14), suggesting that the networks also are less variable (more stagnant) in their alpha-band activity. Even very early in the disease process, close to the emergence of psychosis in the schizophrenia spectrum, distinct distributed cortical networks are impaired and can be detected through aberrant alpha-band network dynamics. These abnormalities were isolated through S-PLVs and NMF and could not be determined using simple whole-brain analyses of alpha power or activity. Thus, NMF holds powerful potential for use on neural data through unbiased identification and isolation of functional networks.

Three of the four abnormal alpha networks were associated with symptoms. From white matter–based connectome analyses, the bilateral cingulate network (network 6) comprises the multimodal cortex and cortical hubs (57) and is one of the rich club areas of the brain (15). Thus, it is perhaps not surprising that resting pathophysiology in this network was associated with overall symptom severity, particularly with thought disorder (Table 2). The left posterior medial and lateral temporal cortex network (network 12) likewise was associated with thought disorder and with overall, positive, and negative symptom severity. The associations of the left posterior temporal cortex and positive symptoms and thinking disturbance in schizophrenia are well documented (58–60), as is the association of medial temporal pathology with paranoia and other psychosis-like symptoms (61,62). The right inferior gyrus hub network (network 13) comprises the right hemisphere analog of Broca's area in the ventrolateral PFC and is thought functionally to serve two main roles: stopping motor responses and inhibiting orienting to distracting stimuli (63,64). Adjacent right BA 47 may be involved in response-reward processing, including delayed reward versus reward magnitude trade-offs and risky choices (65,66). Schizophrenia is associated with increased distractibility and perseveration, likely reflecting some involvement of the right ventrolateral PFC; for example, functional MRI studies in schizophrenia show reduced right inferior frontal gyrus activity on a stop-signal task (67) and reduced coupling of dorsolateral PFC working memory areas and right inferior frontal gyrus (among other PFC areas) when distractors were presented (68). Finally, the bilateral posterior cingulate and superior parietal network (network 14) was associated fairly exclusively with emotional withdrawal. Although both the posterior cingulate and parietal cortex serve as cortical hubs (56) and rich club areas (15), the right parietal lobe is also associated with social behavior and spatial attention. Thus, these networks defined solely on the basis of source-resolved alpha phase locking appear to reflect reasonable physiological networks derived via white matter–based connectomics that are known to be compromised functionally and structurally in schizophrenia. It is reasonable to suggest that dysfunction of alpha communication between distal brain areas may play a role in some of the more complex behavioral symptoms in schizophrenia such as thought disorder. Understanding the network architecture of a biologically validated information carrier frequency (alpha) is an important first step in isolating the systems-level pathophysiology in psychosis.

The analysis in this study is limited by spatially downsampling into BAs to reduce dimensionality. This regional simplification of the brain could explain why alpha activity could be substantially represented with 17 functional networks. The development of improved processing techniques, especially those that would decrease the computation load of S-PLVs and NMF in higher-dimension datasets, would allow for analysis of the brain with less spatial downsampling. This would remove any biases that may be present due to the Brodmann atlas and could potentially facilitate in better localization of neural differences between the subject groups. Methods to perform spectral connectivity across all nodes have been developed (69) and do not suffer from potential issues associated with spatial downsampling. However, accurate functional parcellation of the cortex is needed to translate these purely spatial networks into physiological systems. Currently, we are developing methods to parse the brain based on the Human Connectome Project multimodal functional parcellation (70). This would be a significant improvement over anatomic sulcal-gyral schemes (i.e., Desikan and Destreaux methods) and our gross cytoarchitechtonic approach using downsampled BAs. A major difference between our study and others is that resting-state alpha activity is typically lower in patients with schizophrenia, but that was not the case here. It is possible that differences in alpha power arise later in the disease given that these all were individuals at the first episode of psychosis. However, other studies [e.g., (71)] showed reductions of relative alpha power in EEG at the Cz electrode, suggesting that the abnormality is present early in the disease course. Eyes-open resting activity may identify functional networks that differ from on-task functional networks. Future studies should compare alpha power between eyes-open and eyes-closed conditions as well as between active and passive tasks and should compare EEG and MEG cortical surface resolved measures. Furthermore, such work should investigate changes longitudinally and across the disease course and should compare network segmentation using NMF to other methods such as Graph-ICA (72) on the same MEG dataset. In addition, while the sample size in this study is similar to others in the literature, it limits the statistical significance of the findings and may allow for overfitting of outliers in the model. Although this is a relatively large sample of subjects with FESz (n = 31), it was underpowered for the large number of correlations performed. Thus, caution in interpretation and replication in an independent sample is needed. However, because this is the first study to use NMF to derive data-driven functional networks in alpha activity showing aberrations in subjects with FESz, it is important to examine the full rich set of clinical symptoms in this special sample—1% of the population at its first transition to psychosis. We leave it to the informed reader's discretion to interpret the correlations reported for individual items. Medication may affect brain network function, and we are unable to address that possible confound. Still, participants were only acutely medicated and had less than 2 months of lifetime exposure, so chronic medication effects are unlikely. Future work should assess these possible confounds now that candidate systems have been identified.

Overall, we computationally derived neurophysiological networks that display deficient alpha activity in subjects with FESz. These abnormalities were associated most strongly with overall symptom severity and thought disorder, with the left posterior temporal network also being associated with positive and negative symptom factors. By isolating these irregular networks hidden within the context of undetectable differences in global alpha activity, NMF proves to be a promising tool to isolate communication networks for detailed analyses of systems-level pathophysiology. Using methods that are relatively light computationally, it is possible to identify networks and regions that show selective dynamic abnormalities close to the emergence of psychosis, which may in turn be central to the etiology of psychopathology. These network locations and dynamic abnormalities also provide features to train future data-driven algorithms and guide investigation of pathology in more complex features. Alpha activity, one of the basic carrier frequencies in the brain that establishes distributed cortical circuits, identifies core areas of pathophysiology in the early schizophrenia spectrum.

ACKNOWLEDGMENTS AND DISCLOSURES

This research was supported by National Institutes of Health Conte Center Grant No. P50 MH103204 (David A. Lewis, principal investigator; DFS, project co–principal investigator). HP also received funding from the Swanson School of Engineering and the Office of the Provost at the University of Pittsburgh.

The authors report no biomedical financial interests or potential conflicts of interest.

ARTICLE INFORMATION

From the Department of Bioengineering (HP) and Department of Electrical and Computer Engineering (ES), University of Pittsburgh; Clinical Neurophysiology Research Laboratory (BAC, DFS), Western Psychiatric Institute and Clinic, University of Pittsburgh School of Medicine; and Laboratory of Cognitive Neurodynamics (AG), Department of Neurological Surgery, University of Pittsburgh School of Medicine, Pittsburgh, Pennsylvania.

Address correspondence to Dean F. Salisbury, Ph.D., Clinical Neurophysiology Research Laboratory, 3501 Forbes Ave., Suite 420, Pittsburgh, PA 15213; E-mail: salisburyd@upmc.edu.

Received Feb 20, 2019; revised and accepted Jun 18, 2019.

Supplementary material cited in this article is available online at https://doi.org/10.1016/j.bpsc.2019.06.010.

REFERENCES

1. Salisbury DF, Kuroki N, Kasai K, Shenton ME, McCarley RW (2007): Progressive and interrelated functional and structural evidence of post-onset brain reduction in schizophrenia. Arch Gen Psychiatry 64:521–529.
2. Cropley VL, Klauser P, Lenroot RK, Bruggemann J, Sundram S, Bousman C, *et al.* (2016): Accelerated gray and white matter deterioration with age in schizophrenia. Am J Psychiatry 174:286–295.
3. Dietsche B, Kircher T, Falkenberg I (2017): Structural brain changes in schizophrenia at different stages of the illness: A selective review of longitudinal magnetic resonance imaging studies. Aust N Z J Psychiatry 51:500–508.
4. Andreasen NC (2000): Schizophrenia: The fundamental questions. Brain Res Rev 31:106–112.
5. Friston KJ, Frith CD (1995): Schizophrenia: A disconnection syndrome. Clin Neurosci 3:89–97.
6. Stephan KE, Friston KJ, Frith CD (2009): Dysconnection in schizophrenia: From abnormal synaptic plasticity to failures of self-monitoring. Schizophr Bull 35:509–527.
7. Breakspear M, Terry JR, Friston KJ, Harris AWF, Williams LM, Brown K, *et al.* (2003): A disturbance of nonlinear interdependence in

scalp EEG of subjects with first episode schizophrenia. NeuroImage 20:466–478.
8. Ikezawa K, Ishii R, Iwase M, Kurimoto R, Canuet L, Takahashi H, *et al.* (2011): Decreased alpha event-related synchronization in the left posterior temporal cortex in schizophrenia: A magnetoencephalography-beamformer study. Neurosci Res 71:235–243.
9. Lawrie SM, Buechel C, Whalley HC, Frith CD, Friston KJ, Johnstone EC (2002): Reduced frontotemporal functional connectivity in schizophrenia associated with auditory hallucinations. Biol Psychiatry 51:1008–1011.
10. McGuire PK, Frith CD (1996): Disordered functional connectivity in schizophrenia. Psychol Med 26:663–667.
11. Micheloyannis S, Pachou E, Stam CJ, Breakspear M, Bitsios P, Vourkas M, *et al.* (2006): Small-world networks and disturbed functional connectivity in schizophrenia. Schizophr Res 87:60–66.
12. Fitzsimmons J, Kubicki M, Shenton ME (2013): Review of functional and anatomical brain connectivity findings in schizophrenia. Curr Opin Psychiatry 26:172–187.
13. Kelly S, Jahanshad N, Zalesky A, Kochunov P, Agartz I, Alloza C, *et al.* (2018): Widespread white matter microstructural differences in schizophrenia across 4322 individuals: Results from the ENIGMA Schizophrenia DTI Working Group. Mol Psychiatry 23:1261–1269.
14. Whitford TJ, Grieve SM, Farrow TF, Gomes L, Brennan J, Harris AW, *et al.* (2007): Volumetric white matter abnormalities in first-episode schizophrenia: A longitudinal, tensor-based morphometry study. Am J Psychiatry 164:1082–1089.
15. Van den Heuvel MP, Sporns O (2011): Rich-club organization of the human connectome. J Neurosci 31:15775–15786.
16. Womelsdorf T, Fries P (2007): The role of neuronal synchronization in selective attention. Curr Opin Neurobiol 17:154–160.
17. von Stein A, Sarnthein J (2000): Different frequencies for different scales of cortical integration: From local gamma to long range alpha/theta synchronization. Int J Psychophysiol 38:301–313.
18. Boutros NN, Arfken C, Galderisi S, Warrick J, Pratt G, Iacono W (2008): The status of spectral EEG abnormality as a diagnostic test for schizophrenia. Schizophr Res 99:225–237.
19. Cover KS, Vrenken H, Geurts JJ, van Oosten BW, Jelles B, Polman CH, *et al.* (2006): Multiple sclerosis patients show a highly significant decrease in alpha band interhemispheric synchronization measured using MEG. NeuroImage 29:783–788.
20. Nunez PL, Srinivasan R, Westdorp AF, Wijesinghe RS, Tucker DM, Silberstein RB, Cadusch PJ (1997): EEG coherency: I. Statistics, reference electrode, volume conduction, Laplacians, cortical imaging, and interpretation at multiple scales. Electroencephalogr Clin Neurophysiol 103:499–515.
21. Uhlhaas PJ, Haenschel C, Nikolić D, Singer W (2008): The role of oscillations and synchrony in cortical networks and their putative relevance for the pathophysiology of schizophrenia. Schizophr Bull 34:927–943.
22. Pfurtscheller G (1992): Event-related synchronization (ERS): An electrophysiological correlate of cortical areas at rest. Electroencephalogr Clin Neurophysiol 83:62–69.
23. Pfurtscheller G, Da Silva FL (1999): Event-related EEG/MEG synchronization and desynchronization: Basic principles. Clin Neurophysiol 110:1842–1857.
24. Grabner RH, Fink A, Stipacek A, Neuper C, Neubauer AC (2004): Intelligence and working memory systems: Evidence of neural efficiency in alpha band ERD. Brain Res Cogn Brain Res 20:212–225.
25. Sauseng P, Klimesch W, Doppelmayr M, Pecherstorfer T, Freunberger R, Hanslmayr S (2005): EEG alpha synchronization and functional coupling during top-down processing in a working memory task. Human Brain Mapp 26:148–155.
26. Sauseng P, Klimesch W, Schabus M, Doppelmayr M (2005): Fronto-parietal EEG coherence in theta and upper alpha reflect central executive functions of working memory. Int J Psychophysiol 57:97–103.
27. Benedek M, Bergner S, Könen T, Fink A, Neubauer AC (2011): EEG alpha synchronization is related to top-down processing in convergent and divergent thinking. Neuropsychologia 49:3505–3511.
28. Kerr CE, Sacchet MD, Lazar SW, Moore CI, Jones SR (2013): Mindfulness starts with the body: Somatosensory attention and top-down modulation of cortical alpha rhythms in mindfulness meditation. Front Hum Neurosci 7:12.
29. Palva S, Palva JM (2007): New vistas for α-frequency band oscillations. Trends Neurosci 30:150–158.
30. Samaha J, Bauer P, Cimaroli S, Postle BR (2015): Top-down control of the phase of alpha-band oscillations as a mechanism for temporal prediction. Proc Natl Acad Sci U S A 112:8439–8444.
31. Klimesch W, Sauseng P, Hanslmayr S (2007): EEG alpha oscillations: The inhibition–timing hypothesis. Brain Res Rev 53:63–88.
32. Palva S, Palva JM (2011): Functional roles of alpha-band phase synchronization in local and large-scale cortical networks. Front Psychol 2:204.
33. Buffalo EA, Fries P, Landman R, Buschman TJ, Desimone R (2011): Laminar differences in gamma and alpha coherence in the ventral stream. Proc Natl Acad Sci U S A 108:11262–11267.
34. Spitzer H, Desimone R, Moran J (1988): Increased attention enhances both behavioral and neuronal performance. Science 240:338–340.
35. Gregoriou GG, Gotts SJ, Zhou H, Desimone R (2009): High-frequency, long-range coupling between prefrontal and visual cortex during attention. Science 324:1207–1210.
36. Gregoriou GG, Gotts SJ, Desimone R (2012): Cell-type-specific synchronization of neural activity in FEF with V4 during attention. Neuron 73:581–594.
37. Spaak E, Bonnefond M, Maier A, Leopold DA, Jensen O (2012): Layer-specific entrainment of gamma-band neural activity by the alpha rhythm in monkey visual cortex. Curr Biol 22:2313–2318.
38. Lachaux JP, Rodriguez E, Le Van Quyen M, Lutz A, Martinerie J, Varela FJ (2000): Studying single-trials of phase synchronous activity in the brain. Int J Bifurc Chaos 10:2429–2439.
39. Lee DD, Seung HS (1999): Learning the parts of objects by non-negative matrix factorization. Nature 401:788–791.
40. Brunet JP, Tamayo P, Golub TR, Mesirov JP (2004): Metagenes and molecular pattern discovery using matrix factorization. Proc Natl Acad Sci U S A 101:4164–4169.
41. Virtanen T (2007): Monaural sound source separation by nonnegative matrix factorization with temporal continuity and sparseness criteria. IEEE/ACM Trans Audio Speech Language Process 15:1066–1074.
42. Chai LR, Khambhati AN, Ciric R, Moore TM, Gur RC, Gur RE, *et al.* (2017): Evolution of brain network dynamics in neurodevelopment. Netw Neurosci 1:14–30.
43. Stam CJ, Tavy DLJ, Keunen RWM (1993): Quantification of alpha rhythm desynchronization using the acceleration spectrum entropy of the EEG. Clin Electroencephalogr 24:104–109.
44. Taulu S, Simola J (2006): Spatiotemporal signal space separation method for rejecting nearby interference in MEG measurements. Phys Med Biol 51:1759–1768.
45. Delorme A, Palmer J, Onton J, Oostenveld R, Makeig S (2012): Independent EEG sources are dipolar. PLoS One 7:e30135.
46. Urigüen JA, Garcia-Zapirain B (2015): EEG artifact removal—State-of-the-art and guidelines. J Neural Eng 12:31001.
47. Gramfort A, Luessi M, Larson E, Engemann DA, Strohmeier D, Brodbeck C, *et al.* (2014): MNE software for processing MEG and EEG data. NeuroImage 86:446–460.
48. Lin FH, Witzel T, Ahlfors SP, Stufflebeam SM, Belliveau JW, Hämäläinen MS (2006): Assessing and improving the spatial accuracy in MEG source localization by depth-weighted minimum-norm estimates. NeuroImage 31:160–171.
49. Kabbara A, Falou WE, Khalil M, Wendling F, Hassan M (2017): The dynamic functional core network of the human brain at rest. Sci Rep 7:2936.
50. Ghuman AS, McDaniel JR, Martin A (2011): A wavelet-based method for measuring the oscillatory dynamics of resting-state functional connectivity in MEG. NeuroImage 56:69–77.
51. Kim H, Park H (2007): Sparse non-negative matrix factorizations via alternating non-negativity-constrained least squares for microarray data analysis. Bioinformatics 23:1495–1502.

52. Hutchins LN, Murphy SM, Singh P, Graber JH (2008): Position-dependent motif characterization using non-negative matrix factorization. Bioinformatics 24:2684–2690.
53. Boutsidis C, Gallopoulos E (2008): SVD based initialization: A head start for nonnegative matrix factorization. Pattern Recogn 41:1350–1362.
54. Aviyente S, Bernat EM, Evans WS, Sponheim SR (2011): A phase synchrony measure for quantifying dynamic functional integration in the brain. Hum Brain Mapp 32:80–93.
55. Lachaux JP, Lutz A, Rudrauf D, Cosmelli D, Le Van Quyen M, Martinerie J, Varela F (2002): Estimating the time-course of coherence between single-trial brain signals: An introduction to wavelet coherence. Neurophysiol Clin 32:157–174.
56. Moddemeijer R (1989): On estimation of entropy and mutual information of continuous distributions. Signal Process 16:233–248.
57. Sepulcre J, Liu H, Talukdar T, Martincorena I, Yeo BT, Buckner RL (2010): The organization of local and distant functional connectivity in the human brain. PLoS Comput Biol 6:e1000808.
58. Shenton ME, Kikinis R, Jolesz FA, Pollak SD, LeMay M, Wible CG, *et al.* (1992): Abnormalities of the left temporal lobe and thought disorder in schizophrenia: A quantitative magnetic resonance imaging study. N Engl J Med 327:604–612.
59. Kircher TT, Liddle PF, Brammer MJ, Williams SC, Murray RM, McGuire PK (2001): Neural correlates of formal thought disorder in schizophrenia: Preliminary findings from a functional magnetic resonance imaging study. Arch Gen Psychiatry 58:769–774.
60. Onitsuka T, Shenton ME, Salisbury DF, Dickey CC, Kasai K, Toner SK, *et al.* (2004): Middle and inferior temporal gyrus gray matter volume abnormalities in chronic schizophrenia: An MRI study. Am J Psychiatry 161:1603–1611.
61. Flor-Henry P (1969): Psychosis and temporal lobe epilepsy: A controlled investigation. Epilepsia 10:363–395.
62. Friston KJ, Liddle PF, Frith CD, Hirsch SR, Frackowiak RSJ (1992): The left medial temporal region and schizophrenia: A PET study. Brain 115:367–382.
63. Levy BJ, Wagner AD (2011): Cognitive control and right ventrolateral prefrontal cortex: Reflexive reorienting, motor inhibition, and action updating. Ann N Y Acad Sci 1224:40–62.
64. de Fockert JW, Theeuwes J (2012): Role of frontal cortex in attentional capture by singleton distractors. Brain Cogn 80:367–373.
65. Rogers RD, Owen AM, Middleton HC, Williams EJ, Pickard JD, Sahakian BJ, Robbins TW (1999): Choosing between small, likely rewards and large, unlikely rewards activates inferior and orbital prefrontal cortex. J Neurosci 19:9029–9038.
66. Eshel N, Nelson EE, Blair RJ, Pine DS, Ernst M (2007): Neural substrates of choice selection in adults and adolescents: Development of the ventrolateral prefrontal and anterior cingulate cortices. Neuropsychologia 45:1270–1279.
67. Zandbelt BB, van Buuren M, Kahn RS, Vink M (2011): Reduced proactive inhibition in schizophrenia is related to corticostriatal dysfunction and poor working memory. Biol Psychiatry 70:1151–1158.
68. Anticevic A, Repovs G, Krystal JH, Barch DM (2012): A broken filter: Prefrontal functional connectivity abnormalities in schizophrenia during working memory interference. Schizophr Res 141:8–14.
69. Ghuman AS, van den Honert RN, Huppert TJ, Wallace GL, Martin A (2017): Aberrant oscillatory synchrony is biased toward specific frequencies and processing domains in the autistic brain. Biol Psychiatry Cogn Neurosci Neuroimaging 2:245–252.
70. Glasser MF, Coalson TS, Robinson EC, Hacker CD, Harwell J, Yacoub E, *et al.* (2016): A multi-modal parcellation of human cerebral cortex. Nature 536:171–178.
71. Clementz BA, Sponheim SR, Iacono WG, Beiser M (1994): Resting EEG in first-episode schizophrenia patients, bipolar psychosis patients, and their first-degree relatives. Psychophysiology 31:486–494.
72. Park B, Kim DS, Park HJ (2014): Graph independent component analysis reveals repertoires of intrinsic network components in the human brain. PLoS One 9:e82873.
73. Oostenveld R, Fries P, Maris E, Schoffelen JM (2011): FieldTrip: Open source software for advanced analysis of MEG, EEG, and invasive electrophysiological data. Comput Intell Neurosci 2011:156869.
74. Andreasen NC, Pressler M, Nopoulos P, Miller D, Ho BC (2010): Antipsychotic dose equivalents and dose-years: A standardized method for comparing exposure to different drugs. Biol Psychiatry 67:255–262.
75. Gardner DM, Murphy AL, O'Donnell H, Centorrino F, Baldessarini RJ (2010): International consensus study of antipsychotic dosing. Am J Psychiatry 167:686–693.